communications earth & environment

Article

https://doi.org/10.1038/s43247-024-01472-x

Slab buckling as a driver for rapid oscillations in Indian plate motion and subduction rate

Erik van der Wiel [1,3] ✉, Jakub Pokorný [2,3] ✉, Hana Čížková[2], Wim Spakman [1], Arie P. van den Berg[1] & Douwe J. J. van Hinsbergen [1]

Plate tectonics is primarily driven by the constant gravitational pull of slabs where oceanic lithosphere sinks into the mantle at subduction zones. Under stable plate boundary configurations, changes in plate motion are then thought to occur gradually. Surprisingly, recent high-resolution Indian plate reconstructions revealed rapid (2–3 Million-year) plate velocity oscillations of ±50 %. We show, through numerical experiments, that the buckling of slabs in the mantle transition zone causes such oscillations. This buckling results from the deceleration of slabs as they sink into the lower mantle. The amplitude and period of buckling-associated oscillations depend on average subduction velocity and the available space in the mantle transition zone. The oscillations also affect the upper plate which may explain enigmatic observations of episodic deformation and fluid flow in subduction-related orogens. We infer that the slab pull that drives plate tectonics is generated in just the top few hundred kilometers of the mantle.

Plate kinematic reconstructions provide the quantitative constraints that underpin our understanding of the driving and resisting forces of plate tectonics: primarily slab pull and to a lesser extent ridge push as driving forces[1,2], and mantle drag as either driving or resisting plate motion (particularly by continental keels or slabs), and the resistance on subduction interfaces, as main additional forces[3–5]. An important constraint on plate reconstruction and relative plate motions since the Mesozoic is provided by marine magnetic anomalies that reveal plate motion change on various temporal scales. Reconstructions of major ocean basins usually provide one average Euler pole (plate motion data point) for stages of 3–10 Ma (e.g. ref. 6), even though more magnetic anomalies can be present in such stages. Such reconstructions reveal gradually changing plate motions on tens of millions of year time scales with occasional sudden cusps in plate motion between stages[7–10]. Gradual plate motion changes can be explained by changes in slab pull for example due to slow age variation of subducting lithosphere[11,12], or in the lubrication of plate contacts by a sedimentary cover[3]. Cusps may correspond to changes in contributing forces through e.g., changes in slab pull due to subduction initiation or arrest[13–15], by slab detachment[16] or resistance to subduction of large oceanic plateaus[17], the arrival of a mantle plume-head that may lubricate or push plates[18,19], or to the decrease of a plate area through a breakup (e.g. ref. 20). Only recently, high-resolution (~0.5–1 Ma) plate kinematic reconstructions of India-Africa spreading during the Eocene[21] revealed surprisingly variable ocean spreading kinematics.

It has long been known that the spreading rate between India and Africa, and the convergence rate between India and Asia, between ~65 and ~50 Ma, was very high, close to 20 cm/a[19,22]. Those estimates were based on about one Euler pole every ~5 Ma. White & Lister[23] suspected that shorter-wavelength plate velocity oscillations may have occurred although being smoothed out in existing global plate tectonic reconstructions. Their suspicion was recently corroborated by the high-resolution magnetic anomaly study of DeMets and Merkouriev[21], which revealed that the interval of high India-Asia convergence rate contained rapid oscillations with an amplitude 10 cm/a or more at a period of 6–8 Ma (Fig. 1). Such plate motion variations suggest oscillating changes in either slab pull, or friction on the plate contact with the mantle or the overriding plate, or a combination thereof may become more pronounced with higher rates of subducting plate motion.

Subducting plate motions and changes therein must be accommodated in the underlying mantle. Correlations between imaged mantle structure and the global geological record of subduction show that the remnants of detached slabs in the lower mantle sink with rates of ~1–1.5 cm/a, almost regardless of the rate at which they subducted at a trench[24–26]. Therefore, subducting slabs eventually decelerate from plate tectonic rates (up to 20-25 cm/a[14,27]) to average lower mantle sinking rates of <1.5 cm/a. To accommodate this requires some form of slab shortening or thickening. For instance, seismic tomographic imaging of the lower mantle below India have revealed a major, sufficiently resolved, 'thick' anomaly that is widely

[1]Utrecht University, Utrecht, The Netherlands. [2]Charles University Prague, Prague, Czech Republic. [3]These authors contributed equally: Erik van der Wiel, Jakub Pokorný. ✉e-mail: e.vanderwiel@uu.nl; jaakubpokorny@gmail.com

interpreted to represent the bulk of the Indian plate lithosphere that subducted since the Cretaceous onset of India-Asia convergence, including the lithosphere that subducted between 65 and 50 Ma[28–31]. Its enormous volume represents much of the 8000 km of the India-Asia convergence, and the lithosphere involved must thus have drastically thickened during subduction[25]. Subduction modelling reveals that the deceleration of slabs in the mantle leads to thickening by slab buckling[32,33]. Such buckling behaviour and the resulting stress field in the slab were shown to explain occurrence of earthquakes in the deepest upper mantle[34,35]. Even though the lower mantle tomographic resolution below India cannot resolve the internal buckling structure of the Indian slab remnant, detailed tomographic analyses of slabs in the mantle transition zone and in the top of the lower mantle elsewhere have shown slab buckling in the mantle transition zone[36,37]. Moreover, kinematic reconstruction of those tomographically imaged slabs, through systematic unfolding, reconstructed areas of lost lithosphere that reproduce plate kinematic reconstructions of convergence[36,37]. Such buckling, which potentially may become more pronounced with faster subduction, makes slabs fold backward and forward, creating an oscillating slab dip and slab motion[38–44]. Here, we hypothesize that pronounced slab buckling causes the rapid, large-amplitude Eocene plate motion fluctuations of India.

To test this hypothesis, we conduct numerical experiments with decoupled, freely subducting plates that buckle in the mantle transition zone, creating periodically changing plate motions[45]. We evaluate under which conditions fluctuations such as those reported for the India plate may occur. We will discuss our results in terms of the implications for our understanding of the driving forces of plate tectonics, and how obtaining detailed marine magnetic anomaly records may aid improving the predictive power of plate tectonic reconstructions for applications to plate boundary deformation and magmatic or mineralization processes.

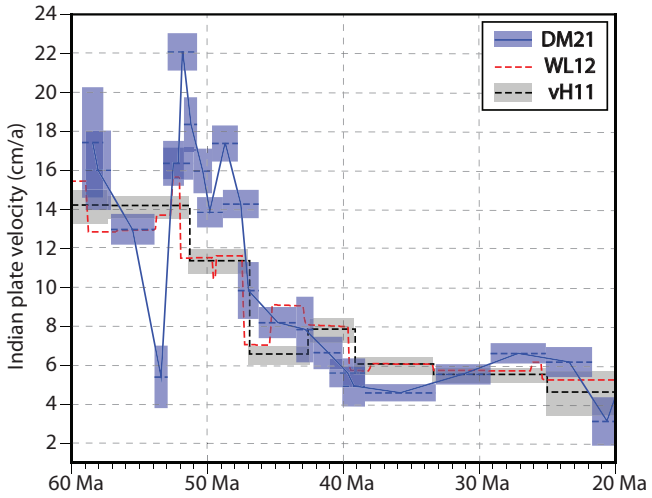

Fig. 1 | Indian plate motion history. Indian plate velocity relative to a fixed Eurasia from 60 Ma ago to 20 Ma ago. Shown are the reconstructed velocities of the Indian plate from DM21[21], WL12[23] and vH11[19]. Blue and grey rectangles indicate error margins in reconstructions and time interval spanned by each stage velocity.

Results

We conducted experiments in a 2D numerical model of subduction (Fig. 2). The rheology of the upper and lower mantle[39,46,47] was chosen to accommodate typical subduction velocities[27] that in the upper mantle exceed the inferred lower mantle slab sinking rates. The average slab sinking rates of 10-15 mm/a[25] are consistent with approximately one order of magnitude viscosity contrast between the lower and upper mantle[46]. This mantle rheology leads to slab shortening and buckling in the upper-to-lower mantle transition zone (MTZ). We experimented with varying lithospheric ages to assess the effect of varying oceanic lithosphere thickness, and with varying crustal viscosities to assess the effect of average plate motion on the amplitude and period of the plate motion. Our slabs have a stress limit of 0.2 GPa and for all the models presented here, we use Clapeyron slopes $\gamma_{410} = 3MPa/K$ and $\gamma_{660} = -1.5MPa/K$. We conducted one group of experiments, with a free overriding plate which leads to slab rollback and results in low angle buckling with multiple buckles[48] (partly) present above the 660 km discontinuity, and lower mantle slab sinking rates (Fig. 3a–g). Another group of experiments implements a fixed overriding plate that suppresses the development of rollback, such that subduction occurs at a mantle-stationary trench (Fig. 3h–n). This generates buckling into a near-vertical slab-pile[49] that slowly sinks into the lower mantle leaving at any time only one buckle present above the 660 km discontinuity.

Slab shortening occurs through the combined resistance of the more viscous lower mantle and the endothermic phase change at the 660 km boundary, while the shallower part of the slab is continuously pulled by the exothermic phase change at 410 km (see methods). Buckling of the shortening slab is then controlled by the non-linear power-law stress limiting mechanism (see methods)[45]. We assess the horizontal velocity of the subducting plate V_{SP} and upper plate V_{UP} as an effect of lithospheric thickness (corresponding to the age of lithosphere at the trench) or through weakening subduction interfaces (crustal viscosity) to evaluate causal relationships between subduction dynamics and oscillating plate motions.

Slab buckling in the reference models

Figure 3 shows two reference experiments for the model setups with and without roll-back. These have a crustal viscosity of $10^{20} Pa \cdot s$ and overriding and subducting plate ages at the trench of 100 Ma. In the model with a mobile overriding plate (Fig. 3 a–g), the slab undergoes a rapid, vertical descent through the upper mantle and the tip of the subducting plate reaches the 660 km discontinuity after approximately 5 Ma model time (Supplementary Movie – panel A). The slab in the transition zone experiences down-dip compression which leads to (nonlinear) rheological weakening, causing the slab to buckle forwards (Fig. 4a) (i.e., towards the overriding plate) over the trapped tip that started to penetrate the 660 km discontinuity. Next, the slab buckles backward (i.e. towards the downgoing plate). This leads to an episode of roll-back and short-lived V_{SP} increase until the slab is

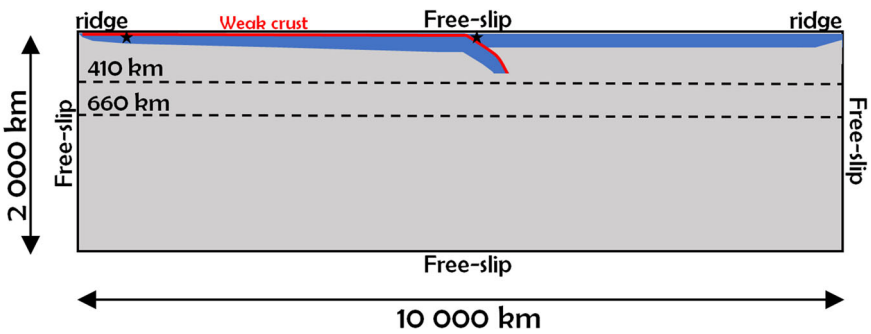

Fig. 2 | Model setup. Model domain is 10,000 km wide and 2000 km deep. Dashed lines indicate major phase transitions at 410 and 660 km depth. The red line positioned at the top of the subducting slab indicates a 10 km thick weak crustal layer, effectively separating the plates. Two black asterisks represent tracers used to track the velocity of the subducting plate and overriding plate. Free slip boundary condition is prescribed on all boundaries.

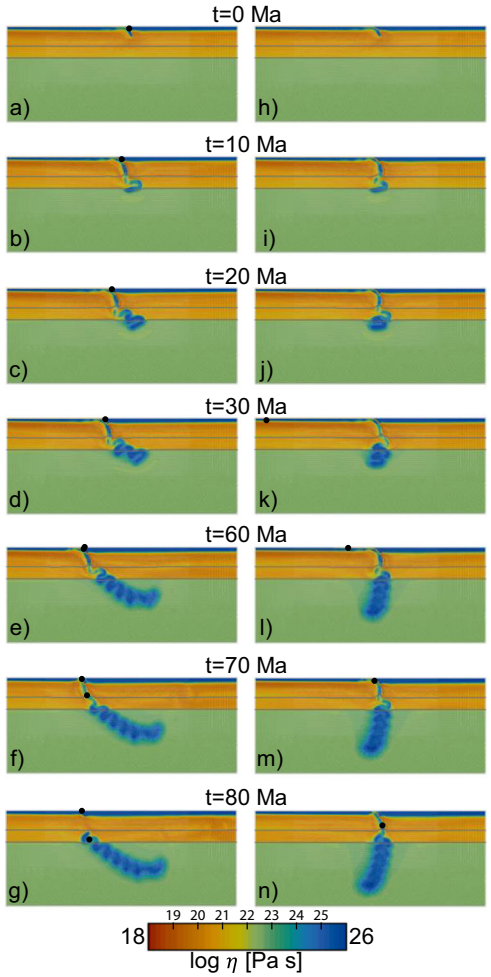

Fig. 3 | Time evolution of the reference models. Zoomed-in viscosity snapshots (4800 × 2000 km) of the model for 80 Ma of model time. Grey lines indicate the position of the major phase transition at 410 and 660 km depth with the values of Clapeyron slopes of 3 and −1.5 MPa/K, respectively. Black dots are reference points used to calculate plate velocities. **a**–**g** Reference model with a free-moving overriding plate resulting in trench retreat and an inclined slab in the lower mantle. **h**–**n** Reference model with a stationary trench creating a vertical lower mantle slab.

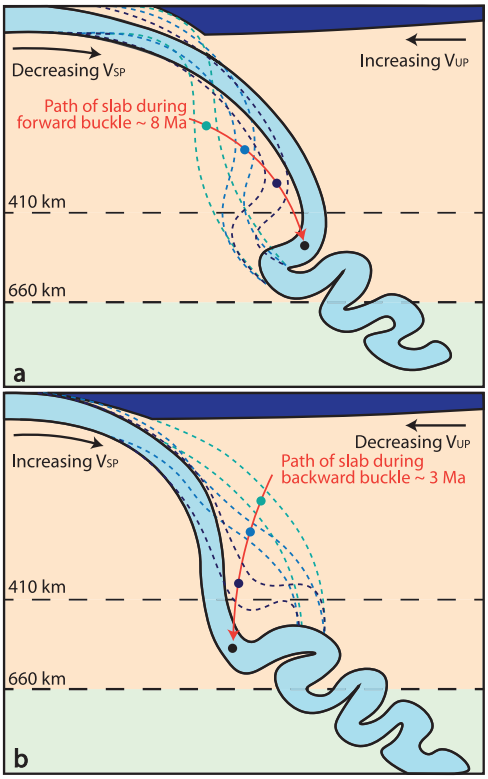

Fig. 4 | Illustrated effect of slab buckling on upper mantle slab geometry. A cartoon illustrating forward (**a**) and backward (**b**) slab buckling as a result of the interplay of the slab with the phase transitions and the lower mantle. During forward buckling the slab in the MTZ advances while the trench retreats, accompanied by a decreasing V_{SP} and increasing V_{UP}. The backward buckle allows the slab to sink fast in the MTZ with a rapid increase of V_{SP}, while the trench stays mantle stationary. The backward buckles form faster than forward buckles, in about 3 versus 8 Ma for our reference model.

almost vertically orientated at $t = 11$ Ma (Fig. 4b). This is followed by the initiation of a second forward buckle, folding the slab over its deeper part in the MTZ, between $t = 11$ Ma and 18 Ma (Supplementary movie – panel A), associated with rollback and a decrease of V_{SP} and increase of V_{UP} (Fig. 4b & 5a). This forward buckle starts tightening at $t = 18$ Ma, inducing the next backward buckle which is followed by a rapid increase of V_{SP} up to 12 cm/a, accompanied by a decrease of V_{UP} to almost 0 cm/a (Fig. 5a). At $t = 20$ Ma the next forward buckle initiated (Fig. 3c), resulting again in an episode of rollback with decreasing V_{SP} and increasing V_{UP} (Fig. 4a & 5a). The characteristic amplitudes of the slab folds in our models (~300–400 km) are consistent with the scaling law for periodic buckling[33,50], being approximately equal to half of the upper mantle thickness.

From here on, this process repeats itself quasi-periodically with new buckles forming approximately every 10 Ma (Fig. 3c–f). This continuous subduction and rollback creates a buckled and thickened slab which slowly enters the lower mantle at an overall low-angle orientation (Fig. 3d–g). After 70 Ma and 5000 km of subduction, the weak crust that facilitates the modelled subduction (see methods) is entirely consumed, the subducting plate is locked to the overriding plate and subduction stops. The modelled slab detaches and sinks into the lower mantle at a rate of ~1 cm/a, on par with inferred and modelled lower mantle slab sinking rates[25,46]. Throughout the experiment, and after 70 Ma of modelled convergence, the overriding plate and trench moved ~1000 km in absolute motion, i.e., relative to the mantle, towards the subducting plate.

The model with a fixed overriding plate, which suppresses rollback (Fig. 3 h-n), shows similar characteristics. The slab is compressed down-dip and rheologically weakened in the transition zone, also resulting in the formation of a second buckle at around t = 10 Ma (Fig. 3i and Supplementary Movie – Panel B). The tightening of the buckle at the base of the upper mantle coincides with an increase in plate velocity around t = 15 Ma (Fig. 5b). Due to the absence of rollback, the buckled slab is oriented vertically, like previously conceptualised 'slab walls'[51]. The oscillations in V_{SP} are of lower amplitude, on the order of 2 cm/a, recurring in a ~12 Ma period (Fig. 5b). Absolute motion rates and oscillations therein of the subducting plate are similar to the scenario with roll-back but because the upper plate is fixed and roll-back does not add to the net convergence rate, subduction continued for ~90 Ma in model time, after which, the modelled slab detached and descended through the lower mantle with similar rate as in the reference model with rollback.

Plate motion oscillations caused by buckling

The quasiperiodic buckling of the subducting plate in the MTZ causes oscillations in the subduction velocity for both types of models (Fig. 5) and in the motion of the overriding plate in the models that allow for roll-back (Fig. 5a). Intervals of fast V_{SP} coincide with tightening of a buckle and steepening of the slab and are followed by a minimum in V_{UP} (Fig. 5). We represent the periodicity of these plate motions with an amplitude and period, which we calculate in a 40 Ma time-interval of steady-state oscillations after subduction initiation and initial descend of the slab to the mantle transition zone, and before the end of the experiment (Fig. 5). In this 40 Ma

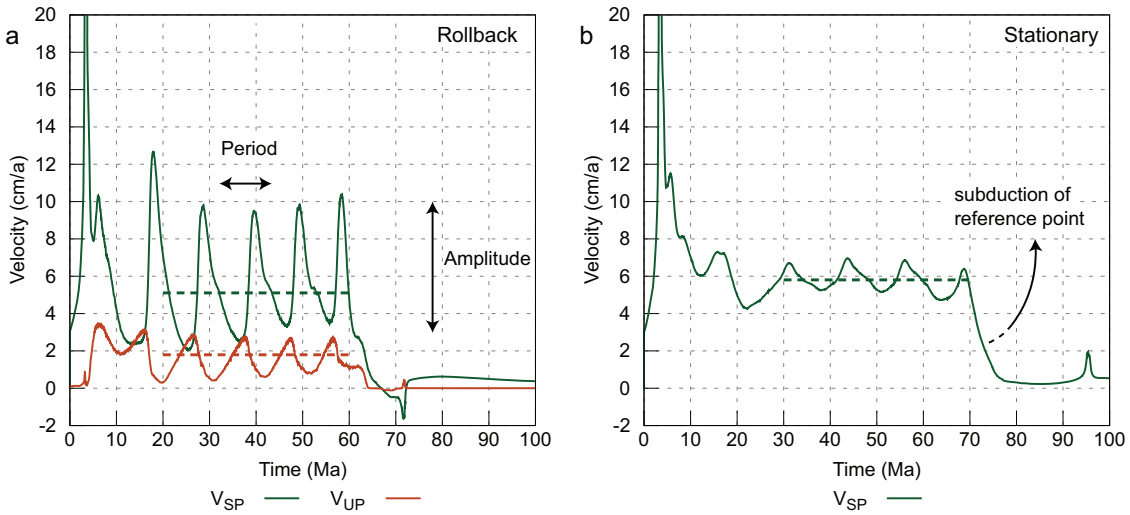

Fig. 5 | Plate motion oscillations. Temporal evolution of the plate motions in both reference models. **a** Subduction velocity and overriding plate motion of the reference model with rollback, V_{SP} oscillates between 2 and 10 cm/a and V_{UP} between 0 and 3 cm/a. The reference point subducts at t = 60 Ma and slab detachment occurs around t = 70 Ma. **b** Similar as in a but for the reference model with a stationary trench, subduction of the reference point occurs at t = 70 Ma and slab detachment at t = 90 Ma. The dashed lines indicate the average velocity, which is calculated over the shown 40 Ma time-interval.

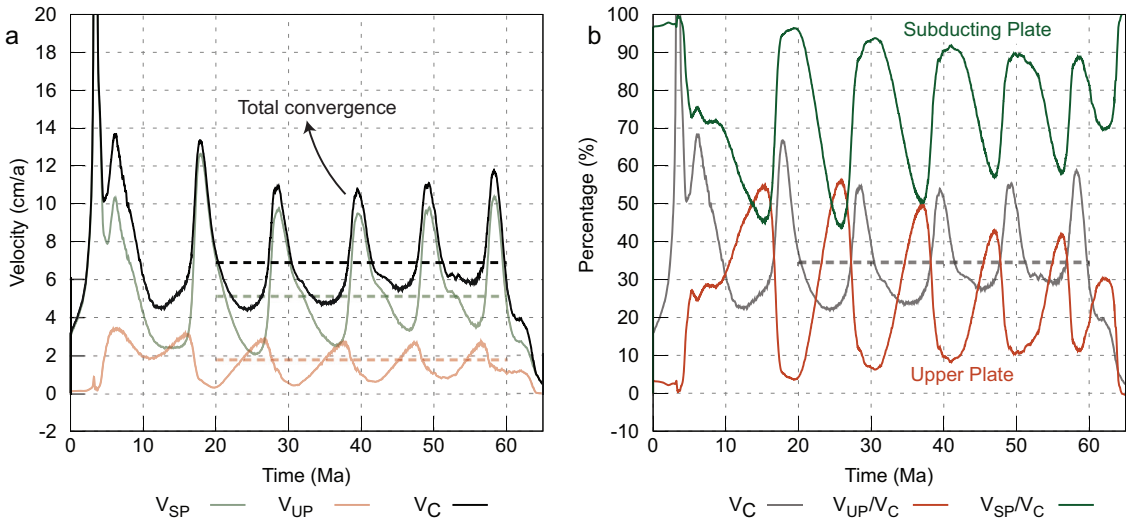

Fig. 6 | Total convergence rate. a Total convergence rate ($V_C = V_{SP} + V_{UP}$) of the reference model with rollback showing smaller amplitudes in the oscillations, red and green lines are the same as in Fig. 5a. **b** Relative percentages of the total convergence rate for both the subducting plate (green; 100-50%) and overriding plate (orange; 50-0%). Grey line is the same as in a, and uses the y-axis of a.

time interval we calculate an average subduction velocity $V_{SP,ave}$ as well as an amplitude and period of oscillations. The amplitude is calculated as the average difference between the maxima and minima of V_{SP}, the period reflects the time for a full buckle to form.

In the reference model with rollback, the subducting plate moved between 20 and 60 Ma with a $V_{SP,ave}$ of 5.1 cm/a while oscillating between ~2 and 10 cm/a (Fig. 5a). The average amplitude and period of the V_{SP} oscillations are 6.8 cm/a and 9.8 Ma (Fig. 5a). Motion of the rigid, undeformable overriding plate, follows the oscillatory motion of the retreating trench. In the 20–60 Ma interval the overriding plate has an average V_{UP} of 1.8 cm/a towards the subducting plate, with oscillations between ~0 and 3 cm/a (Fig. 5a). Maxima in trench motion and V_{UP} coincide with minima in V_{SP}, both occurring during the formation of a new forward buckle and the associated shallowing of slab dip. During tightening of the buckle, the slab rolls back from inclined to vertical, associated with a sharp rise in V_{SP}, this change in angle is associated with a temporally near-stationary trench, and a resulting decrease in V_{UP} towards 0. The total convergence rate (V_C) then also oscillates (Fig. 6a), with an amplitude of 6 cm/a, about 1 cm/a smaller than the amplitude of V_{SP}. The motion of the subducting plate accounts for 50-100% of the total convergence, while the overriding plate is only responsible for 50-0% (Fig. 6b). The highest contribution of trench motion to the convergence occurs during intervals of minimal V_{SP}.

The reference model with a fixed overriding plate (Fig. 3h–n), for which the trench is stationary with respect to the mantle, also shows oscillations in V_{SP} (Fig. 5b) caused by the buckling of the overall vertical slab in the MTZ. In the 40 Ma long time-interval (here, between 30–70 Ma) quasiperiodic buckling occurs with an average V_{SP} of 5.7 cm/a (Fig. 5b), faster than the model with rollback. The oscillations in V_{SP} occur with a period of 12.7 Ma and an amplitude of 1.6 cm/a. This amplitude is more than 4 times lower than the amplitude of oscillations in the model with rollback. The freedom to roll back allows for much larger variation in slab dips, and results in higher amplitudes of plate motion oscillations, as well as a higher net convergence rate.

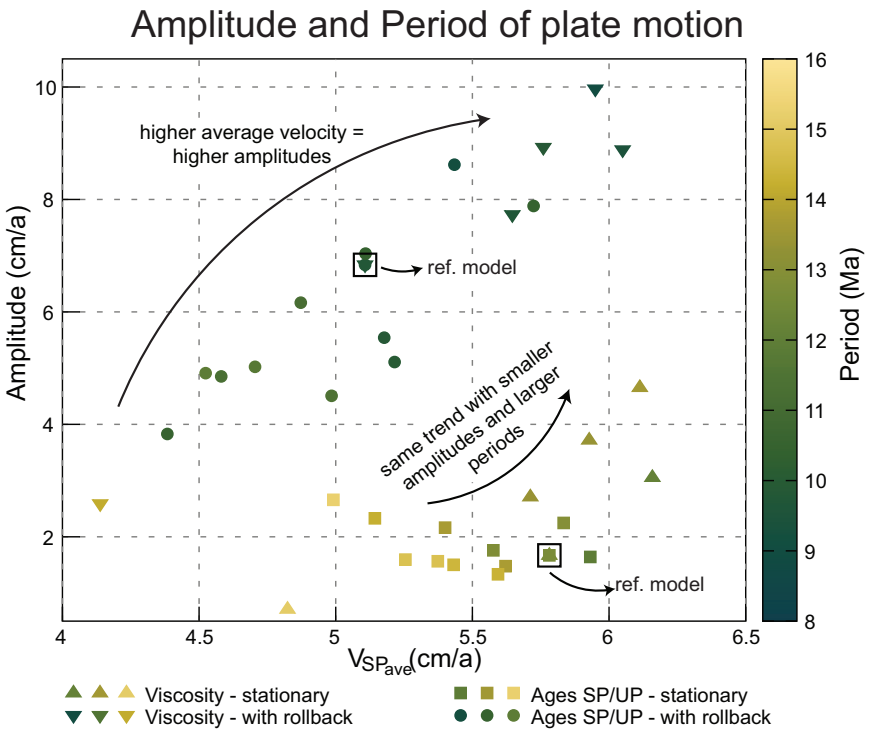

Fig. 7 | Amplitude and Period of the subducting plate motion. Overview of all models showing the relation the amplitude and period (colour) of V_{SP} oscillations have with the average V_{SP}. The four types of models shown are with a varying crustal viscosity and rollback (triangles) or a stationary trench (upside-down triangles), and models with changing SP and UP ages with rollback (circles) or a stationary trench (squares). For values of the crustal viscosity and ages of plates see Fig. 8.

How subduction velocity controls plate motion oscillations

When lithosphere subducts at a rate of $V_{SP,ave} = 5 - 6cm/a$, as in our reference models, it can reach the 660-discontinuity 13–11 Ma after passing the trench. Higher subduction rates decrease that time interval and increase the amount of subducted slab in the MTZ, creating an accommodation space problem. We performed numerical experiments to evaluate the effect of subduction speed on the formation of buckles and on oscillations in V_{SP}. We modified the subduction rate in our experiments in two ways. On the one hand, we performed experiments with constant crustal viscosity while varying the age of the overriding and subducting plates. Overriding plate age determines the length of the subduction interface, with larger interfaces giving more resistance against subduction, decreasing subduction velocity. Subducting plate age determines the negative buoyancy, with higher subduction velocities for older plates[52]. On the other hand, we performed experiments with constant lithosphere ages (100 Ma) while adopting a constant or a power-law crustal viscosity, with lower viscosity yielding higher V_{SP} (e.g. ref. 53; see methods).

In our numerical experiments with varying plate age, the amplitude and period of the oscillations in plate velocity depend on the average subduction velocity (Figs. 7, 8a–f). Models with a younger overriding plate and therefore a shorter subduction interface, have higher average subduction velocities within the 40 Ma long time-interval with steady-state, quasi-periodic buckling (Fig. 8 a, b). These velocities correlate directly to larger amplitudes (2-9 cm/a) in oscillations in the cases with rollback (Fig. 8e). The cases with a stationary trench show that the amplitude of V_{SP} oscillations is predominantly determined by subducting plate age while the effect of the overriding plate age is limited. V_{SP} amplitudes vary between 1–3 cm/a (Fig. 8f). Hence, faster-subducting plates have higher velocity amplitudes and shorter periods of oscillation and, analogous to our reference models, this trend is most profound in models that allow rollback, in which the amplitudes are 2-3 times larger than in models with a mantle-stationary trench (Fig. 7).

The models with a varying crustal viscosity show the same trend: higher average V_{SP}'s leads to larger velocity oscillation amplitudes (Fig. 8c, d) and shorter periods (Fig. 8g, h). Models with a power law crustal viscosity have smaller variations in average V_{SP} between them than those with a constant viscosity and consequently also smaller variations in oscillation amplitudes, albeit with higher absolute amplitudes (Fig. 8 c, d). This is the result of feedback mechanisms between the subducting plate velocity and the strain-rate dependent crustal power law viscosity[45]. Crustal viscosity dynamically responds to changes in slab velocity, where the viscosity decreases as plate velocity (and thus strain-rate) increase. This aids in keeping the period of V_{SP} oscillations constant (Fig. 8g, h).

Discussion

Slabs that subduct with plate motions exceeding the average lower mantle sinking rate of 1–1.5 cm/a[25] inevitably require that slabs shorten and thicken. Interpretations of geophysical observations and subduction models (cited above), including our own, show that this occurs through buckling of the slab in the MTZ (Fig. 3). During slab buckling, the slab dip in the top ~300 km alternates between steep (vertical or overturned) and inclined, and our results illustrate that this induces alternating phases of slab rollback and stagnation (or advance), as well as motion of the trench and upper plate (Fig. 5a). Our results reveal that these alternating phases of forward and backward buckling induce variations in subduction rate and subducting plate motion.

High subduction rates occur in our experiments when the slab buckles backward, towards the downgoing plate and adjacent to a previous slab fold. For backward buckling, the accommodation space in the MTZ in which the buckling slab can sink is available as opposed to forward buckling, in which case the lower part of the MTZ is still occupied by previously buckled slab (Fig. 4a). As the 410 km phase transition enhances the negative buoyancy of slabs and thus enhances slab pull[39] the accommodation in the MTZ for backward buckling allows the slab to force a short (in our reference model <3 Ma) pulse of high V_{SP}, and roll-back. During roll-back, the slab steepens to a vertical orientation accompanied by limited motion of the trench (Fig. 4b), or even trench advance if the upper plate rheology would allow it. Once the slab overturns the next forward buckle initiates, during which time MTZ accommodation space decreases. A forward buckle is associated with trench retreat and slab advance in the MTZ, seemingly rotating over a pivot point in the upper mantle (Fig. 4a). As a result, V_{SP} decreases during a forward buckling slab while V_{UP} increases. As the slab flattens during this forward buckle it creates accommodation space for the next backward buckle and associated acceleration (Fig. 4b). Furthermore, such slab-folding

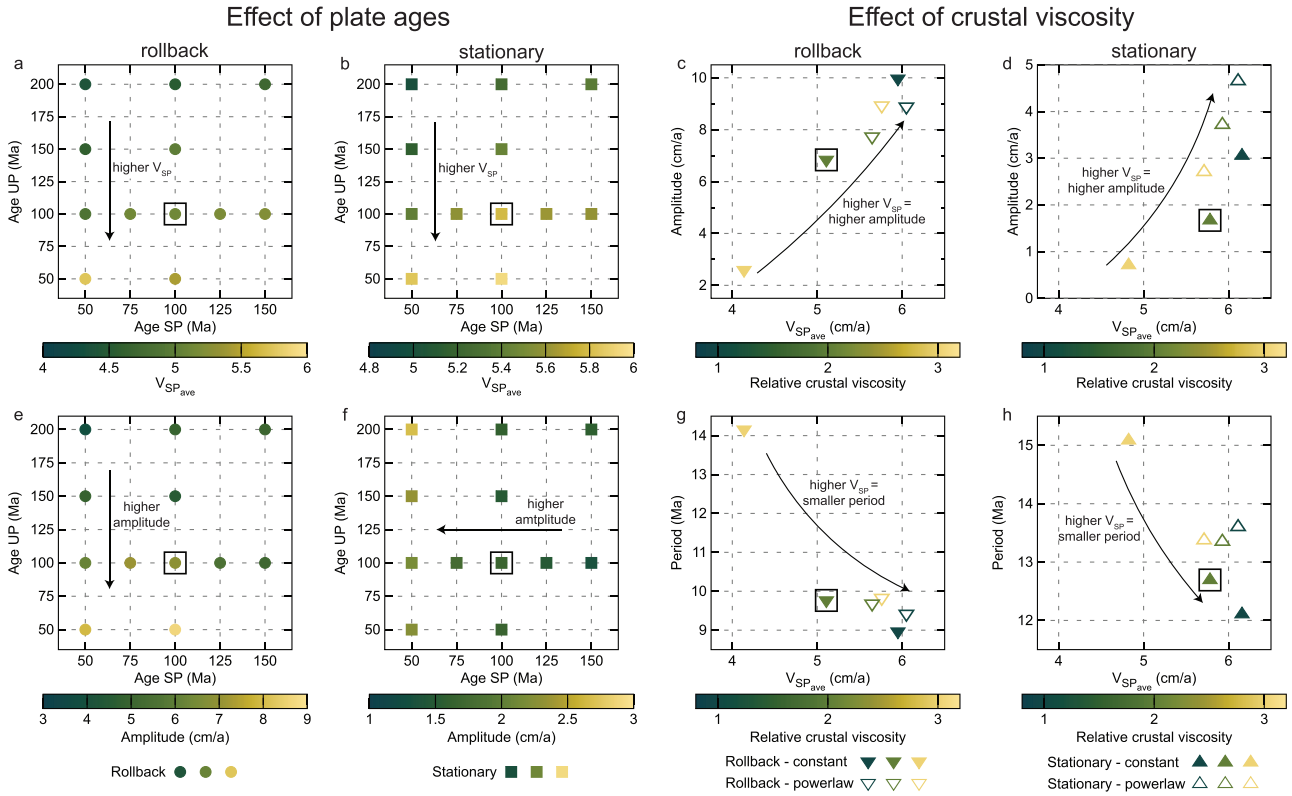

Fig. 8 | Amplitude, period and V_{SP} as function of plate age and crustal viscosity. V_{SP} as function of SP and OP ages for models with a moving trench (**a**) and a stationary trench (**b**). Amplitude of the oscillating V_{SP} as function of the average V_{SP} for crustal viscosities: 5e19, 1e20, 5e20 (closed triangles) and three power law crustal viscosities (open triangles) in models with a moving trench (**c**) and a stationary trench (**d**). Amplitude of the oscillating V_{SP} as function of SP and OP plate ages for models with a moving trench (**e**) and a stationary trench (**f**). Period of the oscillating V_{SP} as function of the average V_{SP} for a varying crustal viscosity in models with a moving trench (**g**) and a stationary trench (**h**).

in the MTZ generates variations in strain-rate in the slab itself which correlate to the occurrence of deep-seismicity in natural subduction zones[34]. The slab-morphologies at varying stages of buckling in our models (Fig. 4) may explain the natural slab-dip variations of present-day subduction zones.

V_{SP} variations in models with a forced stationary trench are smaller because the slab has less variation in the amount of accommodation space in the MTZ. Trench-stationary subduction causes the slab buckling in a vertical column (Fig. 3i–n). Basically, the rate and amplitude of plate motion oscillation primarily depends on the average V_{SP}: the higher, the bigger the space accommodation problem for slab folds in the MTZ. Our experiments with a moving trench and an average V_{SP} of 6 cm/a, i.e., the global average plate velocity[54], reveal rapid oscillations (<10 Ma periods) with large V_{SP} fluctuations (3 to 13 cm/a) (Fig. 6).

Our slab buckling models have shorter periods and larger amplitudes than obtained in previous studies with variations in subduction velocity as a result from slab buckling and eventual slab transfer into the lower mantle[38,39,55–58]. Those previous investigations showed velocity variations of a subducting plate with periods between 15 and 30 Ma owing to smaller subduction plate velocities compared to our models, emphasising the V_{SP} dependency of the oscillations. The trench motion in our models is controlled by the shape of the slab and therefore the interaction between the slab and the MTZ. Imposing a weak asthenospheric layer (WAL) increases subduction rate and decreases trench motion, allowing for a similar lower mantle slab-structure as in our models, especially for young oceanic lithosphere[57]. Therefore, adding a weak asthenospheric layer may increase the subduction rates in our models and even further shorten the period of oscillations while increasing the amplitudes.

The rapid subducting plate motion oscillations that we find in our experiments have similar periods to those recently observed in the high-resolution (0.5–1 Ma) reconstruction of marine magnetic anomalies of the Indian Ocean[21]. Previous plate reconstructions using stage rotations based on larger stage intervals of 5–10 Ma (Fig. 1)[6,19] smoothed out such rapid plate motion changes[23,59]. We illustrate this by sampling V_{SP} in our reference experiment with a mobile upper plate: when we sample on a 1–2 Ma resolution, similar to[21] we resolve rapid (<5 Ma) peaks in plate motion caused by slab buckling (Fig. 9a). However, sampling our V_{SP} curves at larger, typically used intervals of 5 or 10 Ma generates the smooth plate motion history that is widely inferred from plate reconstructions (Fig. 9b, c).

The average V_{SP} as well as the amplitudes of the plate motion oscillations for the case of India are higher than in our experiments. However, a further increase in V_{SP} in our models would probably result in shorter periods and larger amplitudes of oscillation (Fig. 7). The differences between the Indian Plate velocities and our models may be explained by the necessary simplified nature of our models: the absolute plate motion rate of India may have been much higher than we obtained in our experiments because the Indian plate may have been lubricated at the base by a mantle plume[19,60], or the subduction interface may have been lubricated by sediments[3]. The two dimensionality of our models is also unable to characterise the lateral variations in subduction rate of the Indian Plate[19] which may affect the buckling behaviour. Furthermore, the lithosphere in the MTZ during the 55-50 Ma ago interval during which the oscillations were reconstructed may at least partly have been of continental origin[61]. This could have influenced the slab pull, the rate of slab transfer into the lower mantle, and the amount of accommodation space in the MTZ, which would all influence the oscillation V_{SP} amplitude and period in our experiments.

An additional difference with our simplified experiments is that subduction of the Indian plate occurred at a trench that was not retreating, as in our experiments, but instead slowly moving northwards, i.e. advancing[61]. In our experiments, subduction at a mantle-stationary trench occurs with

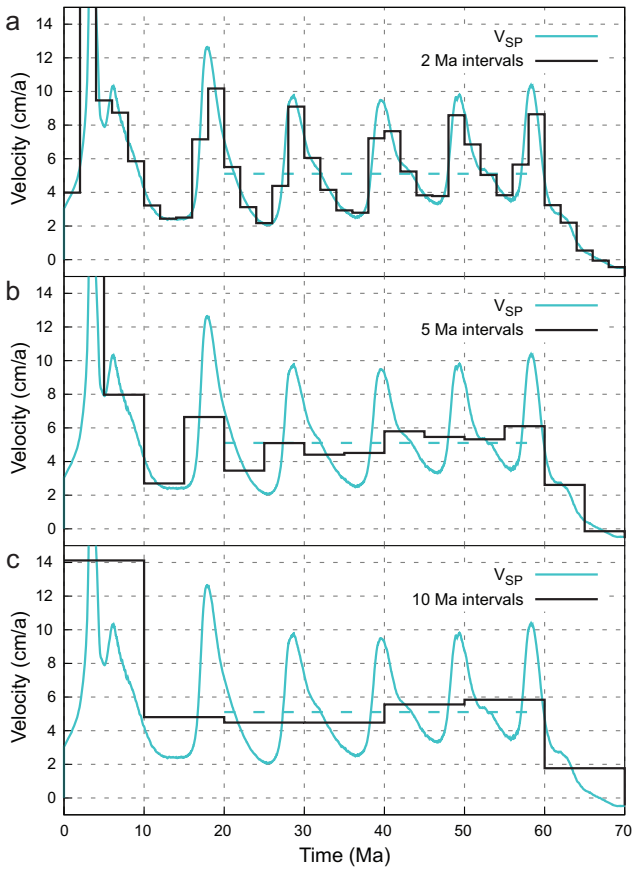

Fig. 9 | Sampling intervals for subducting plate velocity. Horizontal subducting plate motion for the reference model with rollback and stage velocities if sampled at **a** 2, **b** 5 or **c** 10 Ma intervals.

lower amplitude oscillations than those reconstructed by DeMets and Merkouriev[21]. However, the Indian slab may have advanced below the upper plate creating a flat lying slab[61] in which case buckles may form at varying locations below the upper plate which may hamper the effect buckling has on trench motion. Slab buckling combined with trench advance could create an opposite regime as in our experiments, with acceleration during forward buckles and vice versa, as in this case the mantle below the upper plate would have more accommodation space than below the subducting plate. Imposing a thicker or stiffer overriding plate may make a trench more susceptible to advance[62] while slab buckling may then cause the trench to alternate between retreat and advance[63]. We foresee that buckling may produce variations in slab morphology and large variations in subduction rate also when the trench is nearly stationary[57]. With higher subduction rates for India than we reproduced in our experiments, slab buckling must intensify allowing a trench to also advance (besides retreating) which may explain the ~1000 km wide north to south tomographic anomaly widely interpreted as the Indian slab[31] of which we consider its large buckling the plausible and viable candidate to explain the reconstructed Indian Plate velocity oscillations.

In our slab-pull-driven subduction models with a freely moving upper plate we also observe oscillating motion of the trench and upper plate[64]. In our simple experiments, the rigid upper plate is not able to deform, and it thus moves along with the trench where naturally this would lead to changes in stress state, reflected by episodic back-arc spreading[65,66], extensional or contractional upper plate deformation[38,42,67–72] and even changes in topography[56]. Such variations may be of interest to the understanding of fluid and magmatic processes affecting the upper plate. For instance, episodic magmatic ponding alternating with migration and flare ups[73], and episodic mineralization[74] and associated pulses in the formation of ore deposits[75] may be the result of such stress state oscillations. Therefore, for subduction zones where slab buckling leads to oscillating trench motion and upper plate deformation, enhanced resolution in marine magnetic anomalies and accompanying reconstructions could lead to a better predictive power in the timing of these magmatic and ore-genesis-related upper plate processes. In the Andes, alternations on a timescale of ~10 Ma between shortening and trench retreat were recently postulated to result from slab buckling[72]. For Tibet, the only high-resolution deformation records in the relevant time interval of 60-50 Ma ago are from the Qiangtang terrane of northern Tibet, far from the trench[76,77], which on a first order appear to record shortening pulses that coincide with the oscillations[21]. More high-resolution work, for instance in the Xigaze forearc basin, could reveal whether the upper plate may also have recorded short intervals of extension.

Would all subducting plates then show these oscillating plate motions? Higher-resolution tectonic reconstructions could provide the answer, but we see several reasons why not all ridges that border subducting plates may record such oscillations similarly. The process of buckling at long subduction zones might not occur synchronously along the entire trench. Such a process may explain the oscillating azimuth of India-Asia convergence during the documented oscillations[21]. In addition, subduction rate may vary gradually along-strike of a trench (e.g., the west Pacific subduction zones from New Zealand to Kamchatka), and rapidly across triple junctions (e.g. refs. 78,79. Plates like the modern Pacific plate would be less susceptible to the effect of slab buckling in the MTZ, even if the oscillations in a 2D system likely occur. We foresee that oscillations in plate motion are best visible for plates where subduction zones are oriented sub-parallel to spreading ridges and sub-perpendicular to the plate motion direction. Possible candidates for the Cenozoic besides the Indian plate are the Nazca plate[72], the Juan de Fuca plate, the Cocos plate, or the Aluk plate[80] and for earlier times perhaps the Farallon or Kula plates. We consider these targets for high-resolution magnetic anomaly reconstruction to further test the possibilities of slab buckling and the opportunities it may apply to understand mantle and lithosphere dynamics and magmatic and economic geology.

Finally, our models show that the rapid oscillations shown by DeMets and Merkouriev[21] may well be explained by buckling of the subducting slab that results from the accommodation space problem caused by the much lower sinking rates of slabs in the lower mantle. This implies that plate motions that exceed lower mantle slab sinking rates, so larger than 1–1.5 cm/a[24–26], are resisted from the transition zone downwards. In other words, typical plate motions must be primarily driven in the top few hundred kilometers of the mantle. The 410 km phase transition still enhances slab pull, but at the 660 discontinuity the slab encounters resistance and thickens. In addition, the top 100 km of the Earth also resists plate motion due to friction on the subduction interface or drag resistance from the underlying mantle, therefore plate tectonics must primarily be driven between depths of ~100 and 500 km, or only 6–7% of the Earth's radius. This is a remarkably small niche that on Earth apparently has the right conditions for plate tectonics. We foresee that understanding the dynamics of this narrow zone throughout Earth's history holds the key to understand the uniqueness of our planet to start and sustain plate tectonics.

Methods

Model set up

A set of partial differential equations in an extended Boussinesq approximation[81] (EBA) is used to describe our numerical model of subduction. These equations are solved by a finite element method implemented in the SEPRAN package[82,83]. Our model domain is represented by a 2D box 10,000 km wide and 2000 km deep (Fig. 2). The subducting plate stretches from the ridge in the upper left corner to the trench in the middle of the upper surface. The initial temperature distribution in the subducting plate follows a half-space model followed by an adiabatic profile with a potential temperature of 1573 K beneath it.

We carried out two sets of simulations with similar matching parameters. The first set with an overriding plate that is allowed to move freely (subduction with possible rollback), while the second set features a fixed

overriding plate (stationary trench – restricted rollback). Our overriding plate is modelled as a rigid undeformable plate, with a thickness controlled by the thermal age, as there is no evidence for upper plate extension in Tibet. Figure 3 illustrates time evolution of a reference model for both sets of simulations. In these reference models we assume a subducting and overriding plate age of 100 Ma at the trench and the viscosity of the crustal decoupling layer of $10^{20} Pa \cdot s$.

Models of the first set have a mobile overriding plate with a ridge in the upper right corner. The rollback of trench induces the motion of the entire overriding plate towards the left, which is facilitated by the presence of a hot and low-viscosity mid-ocean ridge. The second set of models has a stagnant overriding plate with an age increasing from approximately ~17 Ma at the right-hand side to 100 Ma (i.e., for the reference model) at the trench. Cold and thus strong overriding plates cannot move to the left because of the impermeable free slip condition on the right vertical boundary. Therefore, rollback is prohibited and the trench remains stagnant during the model run. We evaluated the effects of the age of the subducting and overriding plates[40,68] – we tested ages at the trench ranging from 50 Ma to 200 Ma.

To obtain an initial slab with sufficient negative buoyancy that would facilitate subduction, we first execute a short kinematic run to develop the slab tip to a depth of approximately 200 km. Within this kinematic prerun a constant convergence velocity of 2.5 cm/a is prescribed on the top of the subducting plate. After 6 Ma the kinematic boundary condition is turned off and an impermeable free slip is prescribed on all boundaries.

Top and bottom model boundaries are considered isothermal with respective temperatures of 273 K and 2132 K while the vertical boundaries have zero heat flux. Thermal diffusivity is constant $10^{-6}\, m^2\, s^{-1}$ while thermal expansivity is depth dependent[84] and decreases from $3 \times 10^{-5} K^{-1}$ at the surface to $1.2 \times 10^{-5}\, K^{-1}$ at the bottom of the model domain[85].

We consider the major mantle phase transitions: the polymorphous exothermic transition of forsterite to wadsleyite at 410 km depth and the endothermic transition of ringwoodite to bridgmanite and periclase at a depth of 660 km with their associated petrological density contrasts (Supplementary Table 1). These are incorporated through the harmonic parameterization[86] of a phase function[87]. We first performed a parametric study where we varied the values of Clapeyron slopes in a usually accepted range ($\gamma_{410} = 1 - 3$ MPa/K, $\gamma_{660} = -2.5 - (-1.5)$ MPa/K)[88–96]. All these models result in quasiperiodic buckling of the slab, with observed periods of oscillations between ~10-20 Ma. The style of buckling, like the interaction of a slab with the MTZ and the lower mantle, also depends on the strength of the Clapeyron slopes[45,56]. Higher Clapeyron slope for the 410-km phase transition increases slab pull and results in tighter folds while lower Clapeyron slopes reduce the slab pull with fast rollback and as a consequence lead to a lower slab dip[39]. A stronger 660-km phase transition would result in reduced buckling periods. Based on the parametric study we chose a relatively strong $\gamma_{410} = 3MPa/K$ and weak $\gamma_{660} = -1.5MPa/K$ for the phase transitions.

These values were chosen to accommodate realistic subduction behaviour, from subducting plate velocities[27], to the transfer and sinking rates of slabs in the lower mantle, while still agreeing with results from X-ray diffraction experiments and thermodynamic estimates[88–96].

To evaluate the subducting plate velocity and trench retreat velocity in our models we use two passive particles, one initially positioned in the subcrustal lithosphere of the subducting plate (~4600 km left of the trench) and the other one in the overriding plate close to the trench (Fig. 2).

Rheological description

Our subduction model incorporates crustal and mantle material. A low-viscosity crustal layer facilitating mechanical decoupling of the subducting and overriding plate is initially positioned along the top of the subducting plate and within the subduction channel (Fig. 2). Crustal material is tracked using 2 million tracers prescribed in the crust and its closest vicinity. The initial thickness of the crustal layer is 10 km.

Upper mantle material is described by a composite rheology model[97,98] combining dislocation creep, diffusion creep, and a power-law stress limiter which effectively approximates the Peierls creep[99]. In the diffusion and dislocation creep equations (Eqs. 1 and 2), the pressure and temperature dependence of viscosity follows Arrhenius law:

$$\eta_{diff} = {A_{diff}}^{-1} \exp\left(\frac{E_{diff} + pV_{diff}}{RT}\right) \tag{1}$$

$$\eta_{disl} = {A_{disl}}^{-1/n} \dot{\varepsilon}_{||}^{(1-n)/n} \exp\left(\frac{E_{disl} + pV_{disl}}{nRT}\right) \tag{2}$$

$$\eta_y = \sigma_y \dot{\varepsilon}_y^{-(1/n_y)} \dot{\varepsilon}_{||}^{(1/n_y)-1} \tag{3}$$

$$\frac{1}{\eta_{eff}} = \frac{1}{\eta_{diffl}} + \frac{1}{\eta_{disl}} + \frac{1}{\eta_y}. \tag{4}$$

Here $A_{diff/disl}$, $E_{diff/disl,}$, $V_{diff/disl}$ are pre-exponential parameter, activation energy, activation volume for diffusion, and dislocation creep, $\dot{\varepsilon}_{||}$ is the second invariant of the strain rate tensor and n is the power-law exponent of the dislocation creep. A power law stress limiter viscosity is parametrized through the yield stress σ_y, reference strain rate $\dot{\varepsilon}_y$ and a power-law exponent n_y, which is set to 10 in our models (Eq. 3). Assuming unique stress, individual creep mechanism viscosities are combined into the effective viscosity through Eq. 4.

The lower mantle deformation is assumed to be mainly through diffusion creep[100], therefore we take $\eta_{eff} = \eta_{diff}$ in the lower mantle. Prefactor A_{diff} and activation parameters of lower mantle diffusion creep are based fitting the slab sinking rates, reported to be 10-15 mm/a[25]. The viscosity contrast between the lower and upper mantle is about an order of magnitude[46].

The crust in our models is mostly assumed to have constant viscosity in a range of $\eta_c = 5x10^{19} - 5x10^{20} Pa\ s$. We have also conducted several tests with the composite nonlinear rheology of the crust[45] combining dislocation creep[101] and a Byerlee type deformation[102] as an approximation of the brittle failure (pseudoplastic deformation). In these models, dislocation creep viscosity follows Eq. 5 (similar to Eq. 2), but the parameters A_c, E_c, V_c and n_c differ from mantle parameters of Eq. 2 – see table.

$$\eta^c_{disl} = {A_c}^{-1/n_c} \dot{\varepsilon}_{||}^{(1-n_c)/n_c} \exp\left(\frac{E_c + pV_c}{n_c RT}\right) \tag{5}$$

Pseudoplastic deformation limits the maximum stress in the crust to $\sigma^c{}_y$, where this stress limit increases with lithostatic pressure p through Eq. 6, here τ_c is the cohesion and μ is the friction coefficient. The pseudoplastic viscosity η_{pl} is then defined by Eq. 7 and the effective crustal viscosity is given by Eq. 8.

$$\sigma^c{}_y = \tau_c + \mu p, \tag{6}$$

$$\eta_{pl} = \frac{\sigma^c{}_y}{2\dot{\varepsilon}_{||}}. \tag{7}$$

$$\frac{1}{\eta^c{}_{eff}} = \frac{1}{\eta^c{}_{disl}} + \frac{1}{\eta^c{}_{pl}}. \tag{8}$$

Data availability

All modelling data that is used to produce the figures in this manuscript can be found on Zenodo: https://doi.org/10.5281/zenodo.10159525.

Code availability

The code used to run the models can be made available upon reasonable request by Hana Čížková.

Received: 7 December 2023; Accepted: 29 May 2024;
Published online: 12 June 2024

References

1. Forsyth, D. & Uyeda, S. On the relative importance of the driving forces of plate motion. *Geophys. J. Int.* **43**, 163–200 (1975).
2. Lithgow-Bertelloni, C. & Richards, M. A. The dynamics of Cenozoic and Mesozoic plate motions. *Rev. Geophys.* **36**, 27–78 (1998).
3. Behr, W. M. & Becker, T. W. Sediment control on subduction plate speeds. *Earth Planet. Sci. Lett.* **502**, 166–173 (2018).
4. Coltice, N. et al. What drives tectonic plates? *Sci. Adv.* **5**, eaax4295 (2019).
5. Spakman, W. et al. Puzzling features of western Mediterranean tectonics explained by slab dragging. *Nat. Geosci.* **11**, 211–216 (2018).
6. Müller, R. D. et al. A global plate model including lithospheric deformation along major rifts and orogens since the Triassic. *Tectonics* **38**, 1884–1907 (2019).
7. Torsvik, T. H. et al. Global plate motion frames: toward a unified model. *Rev. Geophys.* **46**, 2007RG000227 (2008).
8. Doubrovine, P. V., Steinberger, B. & Torsvik, T. H. Absolute plate motions in a reference frame defined by moving hot spots in the Pacific, Atlantic, and Indian oceans. *J. Geophys. Res.: Solid Earth* **117**, B09101 (2012).
9. Müller, R. D. et al. A tectonic-rules-based mantle reference frame since 1 billion years ago–implications for supercontinent cycles and plate–mantle system evolution. *Solid Earth* **13**, 1127–1159 (2022).
10. Gordon, R. G., Cox, A. & O'Hare, S. Paleomagnetic Euler poles and the apparent polar wander and absolute motion of North America since the Carboniferous. *Tectonics* **3**, 499–537 (1984).
11. Goes, S. et al. Signatures of downgoing plate-buoyancy driven subduction in Cenozoic plate motions. *Phys. Earth Planet. Inter.* **184**, 1–13 (2011).
12. Sdrolias, M. & Müller, R. D. Controls on back-arc basin formation. *Geochemistry, Geophysics, Geosystems* **7**, Q04016 (2006).
13. Gürer, D., Granot, R. & van Hinsbergen, D. J. J. Plate tectonic chain reaction revealed by noise in the Cretaceous quiet zone. *Nat. Geosci.* **15**, 233–239 (2022).
14. Hu, J. et al. Dynamics of the abrupt change in Pacific Plate motion around 50 million years ago. *Nat. Geosci.* **15**, 74–78 (2022).
15. Pusok, A. E. & Stegman, D. R. The convergence history of India-Eurasia records multiple subduction dynamics processes. *Sci. Adv.* **6**, eaaz8681 (2020).
16. Bercovici, D., Schubert, G. & Ricard, Y. Abrupt tectonics and rapid slab detachment with grain damage. *Proc. Natl Acad. Sci.* **112**, 1287–1291 (2015).
17. Knesel, K. M. et al. Rapid change in drift of the Australian plate records collision with Ontong Java plateau. *Nature* **454**, 754–757 (2008).
18. van Hinsbergen, D. J. J. et al. A record of plume-induced plate rotation triggering subduction initiation. *Nat. Geosci.* **14**, 626–630 (2021).
19. van Hinsbergen, D. J. J. et al. Acceleration and deceleration of India-Asia convergence since the Cretaceous: Roles of mantle plumes and continental collision. *J. Geophys. Res.* **116**, B06101 (2011).
20. Wortel, R. & Cloetingh, S. On the origin of the Cocos-Nazca spreading center. *Geology* **9**, 425–430 (1981).
21. DeMets, C. & Merkouriev, S. Detailed reconstructions of India–Somalia Plate motion, 60 Ma to present: implications for Somalia Plate absolute motion and India–Eurasia Plate motion. *Geophys. J. Int.* **227**, 1730–1767 (2021).
22. Patriat, P. & Achache, J. India–Eurasia collision chronology has implications for crustal shortening and driving mechanism of plates. *Nature* **311**, 615–621 (1984).
23. White, L. T. & Lister, G. S. The collision of India with Asia. *J. Geodyn.* **56**, 7–17 (2012).
24. Van Der Meer, D. G. et al. Towards absolute plate motions constrained by lower-mantle slab remnants. *Nat. Geosci.* **3**, 36–40 (2010).
25. van der Meer, D. G., van Hinsbergen, D. J. J. & Spakman, W. Atlas of the underworld: Slab remnants in the mantle, their sinking history, and a new outlook on lower mantle viscosity. *Tectonophysics* **723**, 309–448 (2018).
26. Butterworth, N. et al. Geological, tomographic, kinematic and geodynamic constraints on the dynamics of sinking slabs. *J. Geodyn.* **73**, 1–13 (2014).
27. Zahirovic, S. et al. Tectonic speed limits from plate kinematic reconstructions. *Earth Planet. Sci. Lett.* **418**, 40–52 (2015).
28. Van der Voo, R., Spakman, W. & Bijwaard, H. Tethyan subducted slabs under India. *Earth Planet. Sci. Lett.* **171**, 7–20 (1999).
29. Replumaz, A. et al. 4-D evolution of SE Asia's mantle from geological reconstructions and seismic tomography. *Earth Planet. Sci. Lett.* **221**, 103–115 (2004).
30. Parsons, A. J., Sigloch, K. & Hosseini, K. Australian plate subduction is responsible for Northward Motion of the India-Asia Collision Zone and~ 1,000 km Lateral Migration of the Indian Slab. *Geophys. Res. Lett.* **48**, e2021GL094904 (2021).
31. Qayyum, A. et al. Subduction and slab detachment under moving trenches during ongoing India-Asia convergence. *Geochem., Geophys. Geosyst.* **23**, e2022GC010336 (2022).
32. Goes, S. et al. Subduction-transition zone interaction: A review. *Geosphere* **13**, 644–664 (2017).
33. Ribe, N. M. et al. Buckling instabilities of subducted lithosphere beneath the transition zone. *Earth Planet. Sci. Lett.* **254**, 173–179 (2007).
34. Billen, M. I. Deep slab seismicity limited by rate of deformation in the transition zone. *Sci. Adv.* **6**, eaaz7692 (2020).
35. Pokorný, J. et al. 2D stress rotation in the Tonga subduction region. *Earth Planet. Sci. Lett.* **621**, 118379 (2023).
36. Chen, Y.-W., Wu, J. & Suppe, J. Southward propagation of Nazca subduction along the Andes. *Nature* **565**, 441–447 (2019).
37. Wu, J. et al. Philippine Sea and East Asian plate tectonics since 52 Ma constrained by new subducted slab reconstruction methods. *J. Geophys. Res.: Solid Earth* **121**, 4670–4741 (2016).
38. Billen, M. I. & Arredondo, K. M. Decoupling of plate-asthenosphere motion caused by non-linear viscosity during slab folding in the transition zone. *Phys. Earth Planet. Inter.* **281**, 17–30 (2018).
39. Čížková, H. & Bina, C. R. Effects of mantle and subduction-interface rheologies on slab stagnation and trench rollback. *Earth Planet. Sci. Lett.* **379**, 95–103 (2013).
40. Garel, F. et al. Interaction of subducted slabs with the mantle transition-zone: A regime diagram from 2-D thermo-mechanical models with a mobile trench and an overriding plate. *Geochem., Geophys. Geosyst.* **15**, 1739–1765 (2014).
41. Holt, A. F., Becker, T. & Buffett, B. Trench migration and overriding plate stress in dynamic subduction models. *Geophys. J. Int.* **201**, 172–192 (2015).
42. Lee, C. & King, S. D. Dynamic buckling of subducting slabs reconciles geological and geophysical observations. *Earth Planet. Sci. Lett.* **312**, 360–370 (2011).
43. Schellart, W. P. Influence of the subducting plate velocity on the geometry of the slab and migration of the subduction hinge. *Earth Planet. Sci. Lett.* **231**, 197–219 (2005).
44. Xue, K., Schellart, W. P. & Strak, V. Overriding plate deformation and topography during slab rollback and slab rollover: insights from subduction experiments. *Tectonics* **41**, e2021TC007089 (2022).
45. Pokorný, J., Čížková, H. & van den Berg, A. Feedbacks between subduction dynamics and slab deformation: Combined effects of

nonlinear rheology of a weak decoupling layer and phase transitions. *Phys. Earth Planet. Inter.* **313**, 106679 (2021).
46. Čížková, H. et al. The viscosity of Earth's lower mantle inferred from sinking speed of subducted lithosphere. *Phys. Earth Planet. Inter.* **200**, 56–62 (2012).
47. Čížková, H. & Bina, C. R. Linked influences on slab stagnation: Interplay between lower mantle viscosity structure, phase transitions, and plate coupling. *Earth Planet. Sci. Lett.* **509**, 88–99 (2019).
48. Christensen, U. R. The influence of trench migration on slab penetration into the lower mantle. *Earth Planet. Sci. Lett.* **140**, 27–39 (1996).
49. Běhounková, M. and H. Čížková, Long-wavelength character of subducted slabs in the lower mantle. *Earth Planet. Sci. Lett.* **275**, 43–53 (2008).
50. Ribe, N. M. Periodic folding of viscous sheets. *Phys. Rev. E* **68**, 036305 (2003).
51. Sigloch, K. & Mihalynuk, M. G. Intra-oceanic subduction shaped the assembly of Cordilleran North America. *Nature* **496**, 50–56 (2013).
52. Capitanio, F. et al. Subduction dynamics and the origin of Andean orogeny and the Bolivian orocline. *Nature* **480**, 83–86 (2011).
53. Behr, W. M. et al. The effects of plate interface rheology on subduction kinematics and dynamics. *Geophys. J. Int.* **230**, 796–812 (2022).
54. Van Der Meer, D. G. et al. Plate tectonic controls on atmospheric CO2 levels since the Triassic. *Proc. Natl Acad. Sci.* **111**, 4380–4385 (2014).
55. Gibert, G. et al. Dependency of slab geometry on absolute velocities and conditions for cyclicity: insights from numerical modelling. *Geophys. J. Int.* **189**, 747–760 (2012).
56. Briaud, A. et al. Topographic fingerprint of deep mantle subduction. *J. Geophys. Res.: Solid Earth* **125**, e2019JB017962 (2020).
57. Cerpa, N. G. et al. The effect of a weak asthenospheric layer on surface kinematics, subduction dynamics and slab morphology in the lower mantle. *J. Geophys. Res.: Solid Earth* **127**, e2022JB024494 (2022).
58. Schellart, W. P. et al. Evolution and diversity of subduction zones controlled by slab width. *Nature* **446**, 308–311 (2007).
59. Espinoza, V. & Iaffaldano, G. Rapid absolute plate motion changes inferred from high-resolution relative spreading reconstructions: A case study focusing on the South America plate and its Atlantic/Pacific neighbors. *Earth Planet. Sci. Lett.* **604**, 118009 (2023).
60. Kumar, P. et al. The rapid drift of the Indian tectonic plate. *Nature* **449**, 894–897 (2007).
61. van Hinsbergen, D. J. et al. Reconstructing Greater India: Paleogeographic, kinematic, and geodynamic perspectives. *Tectonophysics* **760**, 69–94 (2019).
62. Sharples, W. et al. Overriding plate controls on subduction evolution. *J. Geophys. Res.: Solid Earth* **119**, 6684–6704 (2014).
63. Stegman, D. R. et al. A regime diagram for subduction styles from 3-D numerical models of free subduction. *Tectonophysics* **483**, 29–45 (2010).
64. Royden, L. H. & Husson, L. Trench motion, slab geometry and viscous stresses in subduction systems. *Geophys. J. Int.* **167**, 881–905 (2006).
65. Ishii, K. & Wallis, S. R. A possible mechanism for spontaneous cyclic back-arc spreading. *Prog. Earth Planet. Sci.* **9**, 27 (2022).
66. Clark, S. R., Stegman, D. & Müller, R. D. Episodicity in back-arc tectonic regimes. *Phys. Earth Planet. Inter.* **171**, 265–279 (2008).
67. Boutoux, A. et al. Slab folding and surface deformation of the Iran mobile belt. *Tectonics* **40**, e2020TC006300 (2021).
68. Capitanio, F. A. et al. Upper plate controls on deep subduction, trench migrations and deformations at convergent margins. *Tectonophysics* **483**, 80–92 (2010).
69. Cerpa, N. G., Guillaume, B. & Martinod, J. The interplay between overriding plate kinematics, slab dip and tectonics. *Geophys. J. Int.* **215**, 1789–1802 (2018).
70. Dasgupta, R., Mandal, N. & Lee, C. Controls of subducting slab dip and age on the extensional versus compressional deformation in the overriding plate. *Tectonophysics* **801**, 228716 (2021).
71. Van Hinsbergen, D. J. & Schouten, T. L. Deciphering paleogeography from orogenic architecture: constructing orogens in a future supercontinent as thought experiment. *Am. J. Sci.* **321**, 955–1031 (2021).
72. Pons, M. et al. Hindered trench migration due to slab steepening controls the formation of the Central Andes. *J. Geophys. Res.: Solid Earth* **127**, e2022JB025229 (2022).
73. Chapman, J. B. et al. The causes of continental arc flare ups and drivers of episodic magmatic activity in Cordilleran orogenic systems. *Lithos* **398**, 106307 (2021).
74. Chelle-Michou, C. et al. High-resolution geochronology of the Coroccohuayco porphyry-skarn deposit, Peru: A rapid product of the Incaic orogeny. *Econ. Geol.* **110**, 423–443 (2015).
75. Wilson, C. J. et al. Structural evolution of the orogenic gold deposits in central Victoria, Australia: The role of regional stress change and the tectonic regime. *Ore Geol. Rev.* **120**, 103390 (2020).
76. Li, S. et al. Does pulsed Tibetan deformation correlate with Indian plate motion changes? *Earth Planet. Sci. Lett.* **536**, 116144 (2020).
77. Li, S. et al. Anisotropy of magnetic susceptibility (AMS) analysis of the Gonjo Basin as an independent constraint to date Tibetan shortening pulses. *Geophys. Res. Lett.* **47**, e2020GL087531 (2020).
78. van de Lagemaat, S. H. et al. Southwest Pacific absolute plate kinematic reconstruction reveals major Cenozoic Tonga-Kermadec slab dragging. *Tectonics* **37**, 2647–2674 (2018).
79. Vaes, B., van Hinsbergen, D. J. J. & Boschman, L. M. Reconstruction of Subduction and Back-Arc Spreading in the NW Pacific and Aleutian Basin: Clues to Causes of Cretaceous and Eocene Plate Reorganizations. *Tectonics* **38**, 1367–1413 (2019).
80. van de Lagemaat, S. H. A. et al. Reconciling the Cretaceous breakup and demise of the Phoenix Plate with East Gondwana orogenesis in New Zealand. *Earth-Sci. Rev.* **236**, 104276 (2023).
81. Ita, J. & King, S. D. Sensitivity of convection with an endothermic phase change to the form of governing equations, initial conditions, boundary conditions, and equation of state. *J. Geophys. Res.: Solid Earth* **99**, 15919–15938 (1994).
82. van den Berg, A., Segal, G. & Yuen, D. A. SEPRAN: A versatile finite-element package for a wide variety of problems in geosciences. *J. Earth Sci.* **26**, 89–95 (2015).
83. Segal, A. and N. Praagman, *The sepran fem package*. Tech. Report, Ingenieursbureau Sepra, Netherlands, 2005.
84. Katsura, T. et al. Thermal expansion of forsterite at high pressures determined by in situ X-ray diffraction: The adiabatic geotherm in the upper mantle. *Phys. Earth Planet. Inter.* **174**, 86–92 (2009).
85. Hansen, U. et al. Dynamical consequences of depth-dependent thermal expansivity and viscosity on mantle circulations and thermal structure. *Phys. earth Planet. Inter.* **77**, 205–223 (1993).
86. Čížková, H., van Hunen, J. & van den Berg, A. Stress distribution within subducting slabs and their deformation in the transition zone. *Phys. Earth Planet. Inter.* **161**, 202–214 (2007).
87. Christensen, U. R. & Yuen, D. A. Layered convection induced by phase transitions. *J. Geophys. Res.: Solid Earth* **90**, 10291–10300 (1985).
88. Morishima, H. et al. The phase boundary between α-and β-Mg_2SiO_4 determined by in situ X-ray observation. *Science* **265**, 1202–1203 (1994).
89. Bina, C. R. & Helffrich, G. Phase transition Clapeyron slopes and transition zone seismic discontinuity topography. *J. Geophys. Res.: Solid Earth* **99**, 15853–15860 (1994).
90. Katsura, T. et al. Olivine-wadsleyite transition in the system (Mg, $Fe)_2SiO_4$. *J. Geophys. Res. Solid Earth* **109**, B02209 (2004).
91. Su, C. et al. Thermodynamic properties of Fe-Bearing Wadsleyite and determination of the Olivine-Wadsleyite phase transition

boundary in (Mg, Fe)$_2$SiO$_4$ System. *Front. Earth Sci.* **10**, 879678 (2022).
92. Litasov, K. et al. In situ X-ray diffraction study of post-spinel transformation in a peridotite mantle: implication for the 660-km discontinuity. *Earth Planet. Sci. Lett.* **238**, 311–328 (2005).
93. Litasov, K. D. et al. Wet subduction versus cold subduction. *Geophys. Res. Lett.* **32**, L13312 (2005).
94. Fei, Y. et al. Experimentally determined postspinel transformation boundary in Mg_2SiO_4 using MgO as an internal pressure standard and its geophysical implications. *J. Geophys. Res. Solid Earth* **109**, B02305 (2004).
95. Katsura, T. et al. Post-spinel transition in Mg_2SiO_4 determined by high P–T in situ X-ray diffractometry. *Phys. Earth Planet. Inter.* **136**, 11–24 (2003).
96. Ishii, T., Kojitani, H. & Akaogi, M. Post-spinel transitions in pyrolite and Mg_2SiO_4 and akimotoite–perovskite transition in MgSiO3: precise comparison by high-pressure high-temperature experiments with multi-sample cell technique. *Earth Planet. Sci. Lett.* **309**, 185–197 (2011).
97. Čížková, H. et al. The influence of rheological weakening and yield stress on the interaction of slabs with the 670 km discontinuity. *Earth Planet. Sci. Lett.* **199**, 447–457 (2002).
98. van den Berg, A. P., van Keken, P. E. & Yuen, D. A. The effects of a composite non-Newtonian and Newtonian rheology on mantle convection. *Geophys. J. Int.* **115**, 62–78 (1993).
99. Androvičová, A., Čížková, H. & van den Berg, A. The effects of rheological decoupling on slab deformation in the Earth's upper mantle. *Stud. Geophys. et. Geodaetica* **57**, 460–481 (2013).
100. Karato, S.-i, Zhang, S. & Wenk, H.-R. Superplasticity in Earth's lower mantle: evidence from seismic anisotropy and rock physics. *Science* **270**, 458–461 (1995).
101. Ranalli, G. *Rheology of the Earth*, 1–414 Springer Science & Business Media, (1995).
102. Karato, S. I. Deformation of earth materials. In *An introduction to the rheology of Solid Earth*, 1–463 (Cambridge University Press, 2008).

Acknowledgements

Netherlands Organisation for Scientific Research, NWO Vici Grant 865.17.001 (EvdW, DJJvH). Charles University Grant Agency, grant number 36121 (JP), grant SVV 260709 (JP, HC). Czech Science Foundation, grant 23-06345S (JP, HC). We thank Craig R. Bina for fruitful discussions and R. Gordon, N. Cerpa and an anonymous reviewer for their constructive feedback and helpful suggestions.

Author contributions

Conceptualization: Evd.W., J.P., D.J.Jv.H. Methodology: EvdW., J.P., H.C., A.PvdB. Investigation: Evd.W., J.P. Visualization: E.vdW., JP Supervision: H.C., D.JJvH Writing – original draft: E.vdW., J.P. Writing – review & editing: Evd.W., J.P., H.C., W.S., A.PvdB., D.J.JvH.

Competing interests

The authors declare no competing interests.

Additional information

Supplementary information The online version contains supplementary material available at https://doi.org/10.1038/s43247-024-01472-x.

Correspondence and requests for materials should be addressed to Erik van der Wiel or Jakub Pokorný.

Peer review information *Communications Earth & Environment* thanks Nestor Cerpa, Richard Gordon and the other, anonymous, reviewer(s) for their contribution to the peer review of this work. Primary Handling Editors: Kim Welford and Carolina Ortiz Guerrero. A peer review file is available.